

# Force-Field Development and Molecular Dynamics Simulations of Ferrocene–Peptide Conjugates as a Scaffold for Hydrogenase Mimics

Xavier de Hatten,<sup>[a, b]</sup> Zoe Cournia,<sup>[c, d]</sup> Ivan Huc,<sup>[b]</sup> Jeremy C. Smith,<sup>[c, e]</sup> and Nils Metzler-Nolte\*<sup>[a]</sup>

**Abstract:** The increasing importance of hydrogenase enzymes in the new energy research field has led us to examine the structure and dynamics of potential hydrogenase mimics, based on a ferrocene–peptide scaffold, using molecular dynamics (MD) simulations. To enable this MD study, a molecular mechanics force field for ferrocene-bearing peptides was developed and implemented in the CHARMM simulation package, thus extending the usefulness of the package into peptide–bioorganometallic chemistry. Using the automated frequency-matching method (AFMM), optimized intramolecular force-field parameters were generated through quantum chemical reference normal modes. The partial charges for ferrocene were derived by fitting point

charges to quantum-chemically computed electrostatic potentials. The force field was tested against experimental X-ray crystal structures of dipeptide derivatives of ferrocene-1,1'-dicarboxylic acid. The calculations reproduce accurately the molecular geometries, including the characteristic  $C_2$ -symmetrical intramolecular hydrogen-bonding pattern, that were stable over 0.1  $\mu$ s MD simulations. The crystal packing properties of ferrocene-1-(D)alanine-(D)proline-1'-(D)alanine-(D)proline were also accurately repro-

duced. The lattice parameters of this crystal were conserved during a 0.1  $\mu$ s MD simulation and match the experimental values almost exactly. Simulations of the peptides in dichloromethane are also in good agreement with experimental NMR and circular dichroism (CD) data in solution. The developed force field was used to perform MD simulations on novel, as yet unsynthesized peptide fragments that surround the active site of [Ni–Fe] hydrogenase. The results of this simulation lead us to propose an improved design for synthetic peptide-based hydrogenase models. The presented MD simulation results of metallocenes thereby provide a convincing validation of our proposal to use ferrocene–peptides as minimal enzyme mimics.

**Keywords:** bioinorganic chemistry • ferrocene bioconjugates • force-field parameterization • hydrogenase mimics • molecular dynamics

## Introduction

Hydrogenases, found in numerous microorganisms, are of particular interest in the field of new energy research, because they catalyze the reversible conversion of dihydrogen

into protons and electrons and thus have potential in hydrogen-based energy generation.<sup>[1–3]</sup> Although biological systems contribute very little to the current energy production, they are capable of substantial large-scale effects. Indeed, the biological processing of dihydrogen performed by hydrogenases is exceptionally efficient, with rates for proton production in the range of 6000–9000 turnovers per second and dihydrogen oxidation of 10000 turnovers per second. Thus,

[a] Dr. X. de Hatten, Prof. Dr. N. Metzler-Nolte  
Department for Chemistry and Biochemistry  
Chair of Inorganic Chemistry I; University of Bochum  
Universitätsstrasse 150, 44809 Bochum (Germany)  
Fax: (+49) 234-32-24153  
E-mail: Nils.Metzler-Nolte@rub.de

[b] Dr. X. de Hatten, Dr. I. Huc  
Université Bordeaux 1–CNRS UMR 5248  
Institut Européen de Chimie et Biologie (IECB)  
2 rue Robert Escarpit, 33607 Pessac (France)

[c] Dr. Z. Cournia, Prof. Dr. J. C. Smith  
IWR-Computational Molecular Biophysics  
University of Heidelberg, Im Neuenheimer Feld 368  
69120 Heidelberg (Germany)

[d] Dr. Z. Cournia  
present address: Chemistry Department, Yale University  
225 Prospect St. CT-06511 New Haven (USA)

[e] Prof. Dr. J. C. Smith  
University of Tennessee and Oak Ridge National Laboratory and  
Center for Molecular Biophysics  
University of Tennessee, 1 Bethel Valley Road  
Oak Ridge, Tennessee 37831 (USA)

 Supporting information for this article is available on the WWW under <http://www.chemeurj.org/> or from the author.

one mole of hydrogenase can, in principle, produce enough hydrogen to fill the airship Graf Zeppelin in ten minutes, or the main liquid-hydrogen tank of the Space Shuttle in two hours.<sup>[2]</sup> This efficiency makes synthetic hydrogenase mimics an attractive target as potential economical sources of hydrogen fuel.

The first structure of a [NiFe]-hydrogenase was solved in 1995.<sup>[4]</sup> Its active site is composed of a hetero-bimetallic center in which a nickel atom is coordinated to four sulfur atoms, two of which are terminal and the other two bridged to an iron atom. In its active form, the iron center is further bonded to three truly inorganic ligands: one carbon monoxide molecule and two cyano groups (see Figure 1). While

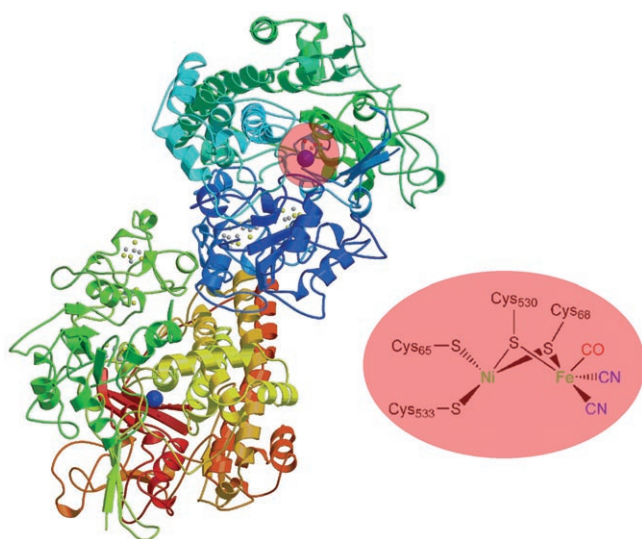


Figure 1. [NiFe]-Hydrogenase enzyme of *Desulfovibrio Gigas* and its heterobimetallic active site. The red selection signifies a magnification.

being ubiquitous in synthetic inorganic chemistry, both ligands are rarely observed to coordinate metal centers in metalloenzymes.

A wide range of different model systems were proposed for the hydrogenase hetero-bimetallic active site.<sup>[5–12]</sup> Out of those, only a few functional models were recently reported.<sup>[13–17]</sup> All of these systems focus on the active site, neglecting the surrounding protein. Also, they use non-proteogenic ligands such as thiophenols, phosphines, or nitrogen ligands. Numerous quantum mechanical computational studies have been carried out that were mainly concerned with the mechanism of dihydrogen binding and activation by the metal centers.<sup>[18–23]</sup> In this work, we propose ferrocene–peptide conjugates as hydrogenase mimics and evaluate their potential as scaffolds for the coordination of bimetallic centers and their synthetic feasibility using molecular dynamics (MD) simulations. Ferrocene–peptide conjugates are anticipated to accurately reproduce the natural active site, because they can simultaneously reproduce the peptidic environment that surrounds the bimetallic center and offer an electron relay.

Hydrogenases are electrochemically active proteins, producing electrons that are subsequently used as reducing equivalents. In peptide-derived hydrogenase mimics, these electrons must first be transferred through the peptide to the site at which the reduction occurs. In the wild type, the electron pathway is directed through [4Fe–4S] clusters.<sup>[24]</sup> We propose that, in synthetic mimics, ferrocene may replace the Fe–S clusters by using the reversible conversion of iron(II) to iron(III) to act as an electron relay.<sup>[25]</sup> Small peptide sequences containing cysteine residues, as in the active site of hydrogenase, can be synthesized and bonded to ferrocene. The complex thus obtained might serve as a chelate for nickel and/or iron atoms, mimicking the [Ni–Fe]-hydrogenase active site. The interactions of metallocenes, and especially of ferrocene, with peptides are becoming of increasing interest.<sup>[26–29]</sup> We<sup>[30–32]</sup> and others<sup>[33–37]</sup> have synthesized a variety of peptide derivatives of ferrocene in order to elucidate the geometries of these compounds and to investigate possible medicinal applications.<sup>[38–43]</sup> In particular, a range of compounds containing ferrocene and cysteine with different protecting groups have been synthesized.<sup>[31]</sup> Interesting geometrical features have been observed in these compounds. Ferrocene is able to induce a turnlike geometry between two short peptides, through novel hydrogen-bonding patterns.<sup>[28,29,39]</sup> Thus, a ferrocene moiety may act both as an electron conductor and as a supramolecular scaffold for the hydrogenase active site.

The application of computational methods to inorganic chemistry has developed at a slower pace than other branches, due to the complexity that arises from modeling ligand field effects in d-block elements.<sup>[44]</sup> Nevertheless, in the present case, a computational approach seemed attractive not only to explore the structures, but also to investigate the dynamics and the stability of new complexes. Most common MD simulation packages, such as CHARMM22,<sup>[45]</sup> are equipped with molecular mechanics (MM) parameter sets for organic biomolecules, but not for transition-metal complexes. Only a few earlier studies have reported the use of CHARMM for the modeling of metallocenes.<sup>[46–48]</sup> An additional fivefold torsion angle had to be introduced by Bosnich and co-workers to model ferrocene.<sup>[46]</sup> Practical implementation of this concept requires modification of the program code to include this new angle. While this concept worked successfully for geometry optimizations of linear and bent metallocenes alone, it is not adaptable to peptide-substituted metallocenes. It thus appeared that no general, transferable parameter set for ferrocene existed in CHARMM prior to this work.

In this paper, the development of a new MM force field for ferrocene-bearing peptides in CHARMM is presented. The force field is tested on independent experimental data including NMR, circular dichroism, and crystal structure data. For the first time, not only the structural, but also dynamical features of potential synthetic models of the hydrogenase active site are explored with MD simulations on metallocenes. Preliminary experimental results for new synthetic models are also presented. This work presents new force-

field parameters for ferrocene that reproduce experimental data in a highly satisfactory way, and it provides proof that ferrocene-peptide conjugates are very promising scaffolds for hydrogenase enzymes, which may serve as an example for metalloenzymes in general.

## Computational Methods

**Molecular structures:** In the present study, nine model systems were simulated (1–9).

The structures of compounds **1** and **2** have been solved crystallographically and were thus chosen to test the parameter set. The initial coordinates were taken from the experimental X-ray structures obtained from the Cambridge Crystallographic Data Centre (CCDC) database.<sup>[49,28]</sup> Compound **3** was crystallized as a diastereoisomer mixture in our laboratory.<sup>[50]</sup> As the crystal structure obtained was a weighted average between two diastereoisomers, MD simulation of the crystalline form is not possible. Consequently, compound **3** was simulated in vacuum. Compound **4** was synthesized and fully characterized in our laboratory, but has not been crystallized yet. Structural information on **4** was obtained from NMR and circular dichroism (CD) spectroscopy, as described later. Model system **5** represents the next synthesis step after compound **4**, involving incorporation of the nickel atom in the sulfur ligand pocket. Model systems **5–9** were chosen so as to identify any unfavorable steric interactions that might hinder the synthesis of these compounds. In model systems **6** and **7**, the ferrocene is bonded to two 6-mer peptides with identical peptide sequences that surround the metal core in the natural active site of the [Ni-Fe] hydrogenase of *Desulfovibrio Gigas*. Systems **8** and **9** were constructed with the same double 6-mer strands as models **6** and **7**, but without including the ferrocene. Two disulfide bridges hold both strands together in model **8** and a nickel atom has the

same role in model **9**. Model systems **4–8** were constructed starting from the crystal structure of Fe-[(L)Ala-(L)Pro]<sub>2</sub> using the graphical interface software Insight II.<sup>[51]</sup> Model **9** was constructed from the crystal structure of hydrogenase from *Desulfovibrio Gigas*<sup>[4]</sup> by isolating the active site, again by using Insight II.

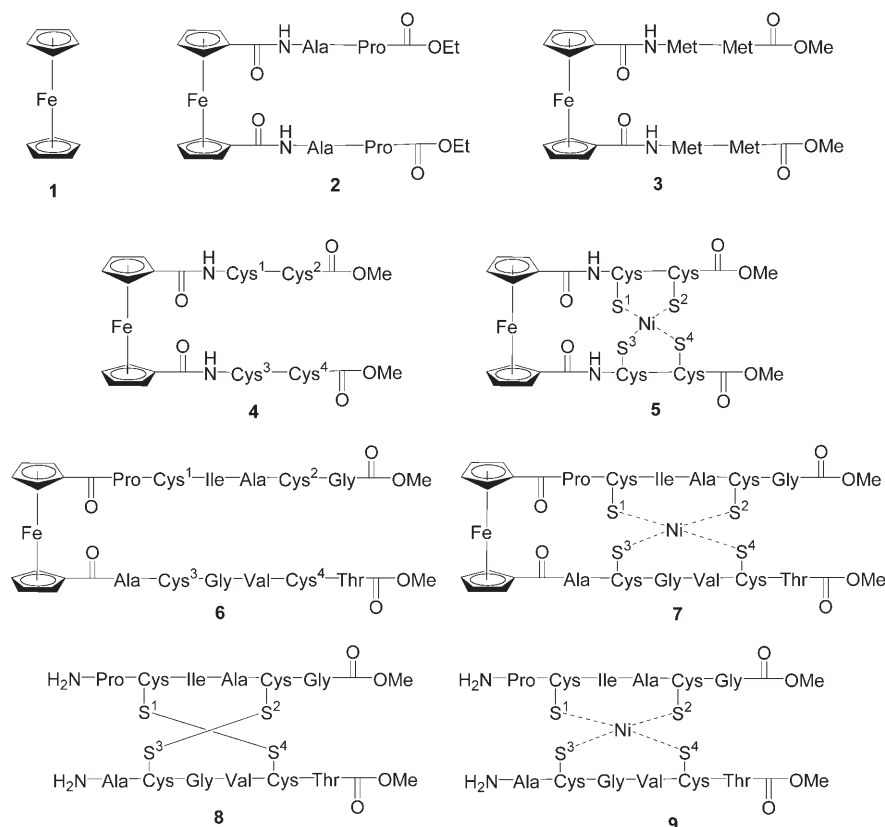
**Computational details:** All molecular mechanics calculations were performed by using the CHARMM22 package, version c27b2. Existing CHARMM force-field parameters were used from reference [52] and the new force-field parameters that were developed here, as described below. All MM minimizations were carried out by using the steepest descent (SD) algorithm for initial minimization; followed by the adopted basis Newton-Raphson (ABNR) minimization<sup>[45]</sup> with a convergence criterion for the energy gradient of 10<sup>-6</sup> kcal mol<sup>-1</sup> Å<sup>-1</sup>. A 13 Å cut-off distance was applied to nonbonded interactions using the CHARMM shifted potential.<sup>[45]</sup>

In CHARMM, the potential energy of a molecule is represented as the sum of contributions from the energy terms associated with bond stretching, angle bending, dihedral rotation, out-of-plane bending, van der Waals, and electrostatic interactions. Equation (1) gives the empirical potential energy function in which  $k_b$ ,  $k_{ub}$ ,  $k_\theta$ ,  $k_\chi$ ,  $k_\psi$  are the bond, Urey-Bradley, angle, dihedral, and improper dihedral force constants, respectively, and  $b$ ,  $s$ ,  $\theta$ ,  $\chi$ ,  $\psi$  the bond lengths, Urey-Bradley 1–3 distances, dihedral angles, and improper torsion angles, respectively.

$$V(r^N) = \sum_{\text{bonds}} k_b (b - b_0)^2 + \sum_{\text{ub}} k_{ub} (s - s_0)^2 + \sum_{\text{angles}} k_\theta (\theta - \theta_0)^2 + \sum_{\text{dihedrals}} k_\chi (1 + \cos(n\chi - \chi_0)) + \sum_{\text{impropers}} k_\psi (\Psi - \Psi_0)^2 + \sum_{\text{nonbonded}} \varepsilon_{ij} \left[ \left( \frac{R_{ij}^{\text{min}}}{r_{ij}} \right)^{12} - 2 \left( \frac{R_{ij}^{\text{min}}}{r_{ij}} \right)^6 \right] + \left( \frac{q_i q_j}{D r_{ij}} \right) \quad (1)$$

Nonbonded interactions between pairs of atoms are described by the Lennard-Jones (LJ) 6–12 term for the van der Waals component and by a Coulomb electrostatic interaction. The terms  $R_{ij}^{\text{min}}$  and  $\varepsilon_{ij}$  are the distance between atom  $i$  and  $j$  at which the Lennard-Jones is at potential minimum and the depth of the potential well for the same pair of atoms, respectively.  $D$  is the effective dielectric constant which was set to 1 and  $q_i$  is the partial charge on atom  $i$ . Where missing, hydrogen atoms were constructed by using idealized geometric parameters from the HBUILD module in CHARMM.<sup>[53]</sup>

All quantum mechanical (QM) calculations were performed with the NWChem 4.5 package.<sup>[54]</sup> The Hartree-Fock and the MP2 levels of theory provide poor results for the description of metallocenes.<sup>[55]</sup> On the other hand, DFT calculations have been shown to give accurate results in the optimization of metallocene geometries.<sup>[56]</sup> Therefore, the structure optimizations and normal mode analyses of ferrocene and of ferrocene-1-(L)alanine-1'-(L)proline in vacuum were performed by using the DFT/B3LYP level of theory with a double-zeta valence basis plus double-polarization (DZVP2).<sup>[57]</sup> The geometry optimizations were performed to a maximum gradient of 0.00045 a.u. and a root-mean-square (rms) gradient of 0.0003 a.u. in Cartesian coordinates. The frequencies were calculated nu-



merically. A frequency scaling of 0.97 was used to compensate for the use of the harmonic approximation to the potential-energy surface.<sup>[58]</sup>

The partial atomic charges were calculated for the ferrocene structure with the CHELPG method<sup>[59]</sup> on the DZVP2-optimized structure. CHELPG employs a least-squares fitting procedure to determine the set of atomic partial charges that best reproduces the quantum mechanical electrostatic potential at selected grid points. The grid was extended to 3 Å from any of the atomic centers and the grid spacing was set to 0.1 Å. The grid points for which the QM electrostatic potential was evaluated and used in the fitting procedure of the partial atomic charges all lie outside the van der Waals radii of the atoms and within a cutoff distance from the atomic centers: in this study, all grid points lying within a distance of less than 2 Å from any of the atomic centers were discarded. The fitting was subjected to the constraint that the sum of the charges should be equal to the net charge on the molecule. To ensure that the charges on symmetrically equivalent atoms are equal, additional constraints on the partial atomic charges were imposed during the fitting procedure: the iron was constrained to have a charge of +2 and each of the cyclopentadienyl groups were constrained to have a total charge of -1.

Following energy minimizations, the MD simulations were performed with the Verlet algorithm<sup>[59]</sup> with integration time steps of 0.001 ps. For the isolated molecule calculations, MD simulations were performed on the model systems (1–9) in the microcanonical (NVE) ensemble. Initially, the systems were heated to room temperature (298 K) in 5 K temperature increments. Then, equilibration for 10 ps with velocity rescaling followed, with a second phase of equilibration without velocity rescaling for another 10 ps at the same temperature. Finally, production dynamics followed at 298 K. The length of the calculations depends on the size of the system. Simulations were performed over 1 μs for the single molecules in vacuum, 0.5 μs for the single molecules in explicit solvent, and 0.1 μs for the molecules in the crystalline state.

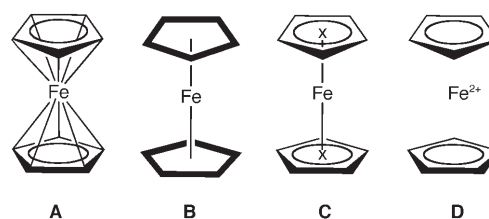
For calculations including the crystal environments, the MD simulations were performed at constant pressure and temperature with periodic boundary conditions in all directions. Starting from experimental coordinates and after minimization, the system was heated to the desired temperature in 5 K steps. Subsequently, the structures were equilibrated for 50 ps at this temperature by using velocity rescaling followed by a second phase of equilibration without velocity rescaling for another 10 ps. Finally, production dynamics followed for 100 ns for the ferrocene-1-(D)alanine-(D)proline-1'-(D)alanine-(D)proline crystal and 10 ns for the ferrocene crystal. The unit-cell dimensions were allowed to vary during both the energy minimization and the MD calculation.

For the calculations including explicit solvent molecules, a CH<sub>2</sub>Cl<sub>2</sub> box was created. Dichloromethane has been previously parameterized in CHARMM only for use with the united-atom force field. Here, we have used an all-atom dichloromethane and the missing intramolecular parameters were calculated from an automated frequency matching method (AFMM) calculation, which is described below. For the solvation calculation, the solute was solvated by overlaying a 25.14 Å orthorhombic box of CH<sub>2</sub>Cl<sub>2</sub> and deleting all solvent molecules which were either outside a sphere with a 16 Å radius centered on the geometric center of the solute or overlapping a solute atom; a solvent molecule is regarded as overlapping a solute atom if one of its atoms, either C or Cl is within 2.8 Å of the another. The final systems contained one solute and 140 solvent molecules in the case of compound 2 and one solute and 142 solvent molecules in the case of compound 4. The stochastic boundary molecular dynamics (SBMD) method was used for all simulations in explicit solvent.<sup>[52]</sup> For calculations including the solvent molecules, MD simulations were performed at constant pressure and temperature. Starting from experimental coordinates for the solute and for the solvent, the system was first minimized and then heated to 295 K (room temperature) in 5 K steps. Subsequently, the structures were equilibrated for 50 ps at this temperature using velocity rescaling followed by a second phase of equilibration without velocity rescaling for another 10 ps. Finally, production dynamics followed for 500 ns.

**Ferrocene topology:** The topology of bis-cyclopentadienyl complexes of the type [M(Cp)<sub>2</sub>]<sup>n+</sup> requires the description of the metal–ligand π-bond.

Four different approaches have been used in the literature to model ferrocene with molecular mechanics.

The first method uses ten harmonic restraints connecting each carbon atom of the Cp ring to the iron center (A).<sup>[61]</sup> The second “rigid-body” approach treats the Cp ligand as a rigid single pentagonal unit (B). The



third method introduces a massless “dummy” atom (X) placed at the center of geometry of each of the Cp rings (C). The metal is connected with a spring to the dummy atom, which is in turn connected with springs to the five carbon atoms around it. This dummy atom approach has been shown to give fairly accurate results for ferrocene simulations using CHARMM.<sup>[62]</sup> However, unrealistic force constants are needed to maintain the dummy atom at the centroid during minimization and spurious vibrational modes are generated when the force field is used to calculate vibrational spectra.<sup>[46]</sup> The last method is a nonbonded approach in which the cyclopentadienyl aromatic moieties and an Fe<sup>2+</sup> ion are held together by electrostatic and van der Waals interactions (D).<sup>[47]</sup>

In the present work, a modified electrostatic model (D) was implemented. It is known that, due to the particular partly-covalent nature of the d-block metal–carbon bonds,<sup>[63]</sup> the forces that maintain ferrocene cannot be solely described by Coulombic electrostatic interactions. Since current force fields are unable to quantitatively describe the metal–ligand bond, an additional constraint is required. Therefore, in the present model the substituted Cp rings and the iron atom interact with each other with both nonbonded terms and also distance restraints that hold together the Cp rings and the iron atom. The CHARMM potential energy has a restraint term that prevents large motions of individual atoms. In the present case, all carbon atoms on the Cp rings were constrained to be equidistant from the central iron (2.05 Å) with a harmonic constraint force constant of 100 kcal mol<sup>-1</sup> Å<sup>-2</sup>. Our model reproduces the key features of ferrocene in that it 1) keeps the fivefold symmetry of a metal–Cp unit, 2) allows for rotation about the metal–Cp(centroid) bond, and 3) keeps the two Cp rings at the optimized distance at all times during the calculations.

**Nickel core topology:** For the models containing nickel, harmonic restraints were introduced between each of the four sulfur atoms and the nickel atom. The four sulfur atoms were constrained to be equidistant from the nickel core (2.25 Å) by using 10 kcal mol<sup>-1</sup> Å<sup>-2</sup> harmonic constraints. It was found that for model system 9, which contains the nickel portion of the bimetallic active site of [NiFe]-hydrogenase, no additional restraint was needed to hold the nickel atom in the chelating pocket; the MM Coulombic electrostatic attraction was sufficient. No effort was made to simulate a particular ligand field for the d<sup>8</sup>-Ni ion.

**Parameter refinement:** The reliability of an MM calculation is dependent on the functional form of the potential-energy function and on the numerical values of the parameters incorporated in it. Therefore, the values of the various parameters in Equation (1) had to be determined. For the derivation of the missing intramolecular parameters we used the AFMM method.<sup>[64]</sup> AFMM optimizes the parameters by adjusting the eigenvalues and eigenvectors of normal modes calculated with CHARMM to fit the normal modes calculated with high-level quantum chemistry methods. This method has been successfully used to derive parameters for a range of biologically-important compounds.<sup>[65–68]</sup>

An efficient way to check simultaneously for both eigenvector orthonormality and frequency matching is to project each of the CHARMM eigenvectors onto the reference set of QM eigenvectors, to find the frequency ( $\nu_j^{\max}$ ) that corresponds to the highest overlap, and to compare this frequency with the corresponding QM frequency ( $\nu_j$ ). In the ideal

case  $\nu_i = \nu_i^{\max}$  and  $\bar{\chi}_i^M \bar{\chi}_i^O = \delta_{ij}$  (in which  $\delta_{ij}$  is the Kronecker delta,  $\bar{\chi}_i^M$  is the set of the MM eigenvectors and  $\bar{\chi}_i^O$  is the reference set of QM eigenvectors). AFMM is based on iteratively minimizing the sum-of-squares ( $Y^2$ ) of the deviations from the ideal situation as given by Equation (2) in which  $N$  is the number of atoms in the molecule and there are  $3N-6$  independent vibrational frequencies.

$$Y^2 = \sum_{3N-6} (\nu_i - \nu_i^{\max})^2 \quad (2)$$

The LJ parameters  $\epsilon_{ij}^{\min}$  and  $R_{ij}^{\min}$  [see Eq. (1)] depend mostly on the atomic properties and are relatively insensitive to changes in the molecular environment. Here, these were directly transferred from original CHARMM values and were not modified during refinement. Iron has been parameterized in CHARMM and has been implemented in numerous heme calculations.<sup>[69,70]</sup> However, in CHARMM, the  $\epsilon$  value of the LJ potential, which governs the depth of the potential well, was set to zero so as to avoid unwanted repulsive interactions between the iron and the heme group. This approximation, although valid within the heme group, cannot be used in the present study, in which both the repulsive and attractive van der Waals interactions within the ferrocene play important roles. Sets of nonbonded parameters for the iron and nickel were supplied by Bredenber.<sup>[71]</sup> Nickel can adopt various geometries,<sup>[73-79]</sup> but for the current study, only the conformation that is in the hydrogenase active site was taken into account.<sup>[72]</sup> Equilibrium values for bonds ( $b_0$ ), angles ( $\theta_0$ ) and dihedrals ( $\chi_0$ ) that were not existing in the original CHARMM force-field parameter set<sup>[80,81]</sup> were determined from the protein crystal structure and were not further optimized. Before refinement of the unknown parameters, an initial set of parameters was determined, based on similar, already-existing CHARMM parameters and on chemical intuition, carefully considering the equilibrium values and hybridization of the atoms.

A desirable property of an MM force field is the transferability of the parameter set. Therefore, when designing a new parameter set, the addition of new atom types to the force field should be limited to those specific cases in which existing type cannot be used. Because of the particular geometry of the present ferrocene compounds and the characteristic distribution of the partial charges of the atoms along the Cp rings, it was found necessary to introduce a new CHARMM atom type (CA2) for the carbon atoms in ferrocene belonging to five-membered aromatic rings (see Figure 2a). The van der Waals parameters for the type CA2 were taken to be the same as those for aromatic carbon atoms (type CA). The nickel atom type (Ni) also did not exist in CHARMM and was therefore added with a partial charge of +2 corresponding to its formal charge in these types of complexes. For the hydrogen atoms of the Cp ring, the existing atom type HP was used with a modified partial charge (see Supporting Information) as calculated from QM. The charge of the oxygen atoms on the carbonyl group of the first amide bond connected to ferrocene was changed from  $-0.51$  to  $-0.61$  so as to maintain the total charge at  $-1$  for the Cp-ring residue (FEC residue, see Supporting Information). For the nickel coordination center, the existing cysteine residue (CYS) was used as a starting point to develop a new cysteine residue (CYN) (see Supporting Information), which was adapted to represent a cysteine that can accommodate a coordinating bond with nickel. This residue was used only for the model systems containing nickel. In the CYN residue the hydrogen atom of the thiol group was removed and thus the total charge for this residue was set to  $-0.50$ . The rest of the negative charge was transferred to the sulfur atom, the charge of which was set to  $-0.57$ . It was therefore necessary to determine new parameters also for the energy terms involving the newly created atom types.

For the automated parameter refinement, the geometry of the compounds Fc-1-Ala-1'-Pro (Figure 2) and  $\text{CH}_2\text{Cl}_2$  were optimized as described below. During the automated frequency matching the range over which force constants were allowed to vary was  $10\text{--}500 \text{ kcal mol}^{-1} \text{ \AA}^{-2}$  for bonds,  $1\text{--}200 \text{ kcal mol}^{-1} \text{ rad}^{-2}$  for angles,  $0.1\text{--}100 \text{ kcal mol}^{-1}$  for dihedrals, and  $0.1\text{--}100 \text{ kcal mol}^{-1} \text{ rad}^{-2}$  for improper torsion angles. It was observed that by restarting the calculation with the optimized force constants that were obtained from the previous optimization step and by limiting the range each time around the new optimized parameter value, the normal-

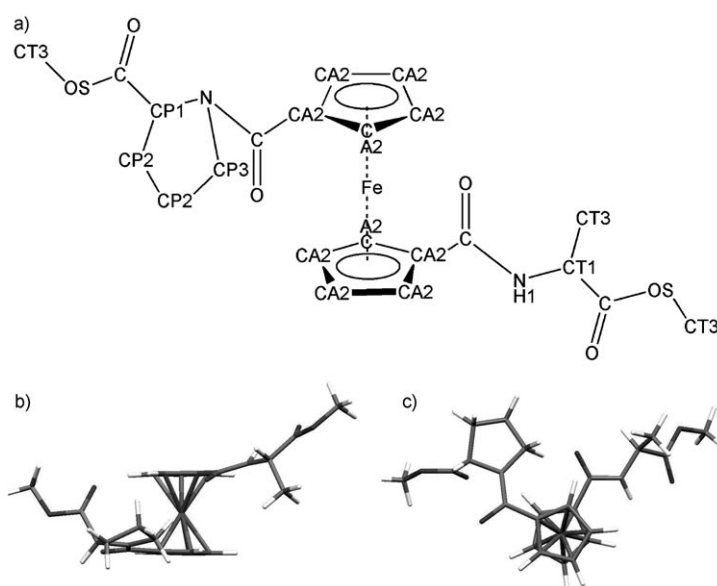


Figure 2. a) Topology scheme of ferrocene-1-proline-1'-alanine showing the CHARMM atom types. b) and c) Its DFT/B3LYP energy-minimized structure of ferrocene-1-(L)proline-1'-(L)alanine viewed along the  $b$  and the  $c$  axes, respectively.

mode matching was significantly improved. In this manner, the optimizations for all force constants were ran four times. For the first run the convergence of the function  $Y^2$  was set to 10000 steps. The last three optimizations were allowed to run until the value of  $Y^2$  remained constant for at least 1000 steps. The root-mean-square deviation ( $\sigma$ ) from the reference case was evaluated at the end of the calculation [Eq. (3)].

$$\sigma = \sqrt{\frac{\sum_{3N-6} (\nu_i - \nu_i^{\max})^2}{3N-6}} \quad (3)$$

## Results and Discussion

**Parameterization of ferrocene-1(L)proline-1'(L)alanine:** For the synthesis of ferrocene-bearing peptides, ferrocene 1,1'-dicarboxylic acid is often linked to the N termini of two amino acids through a peptide bond. This special peptide bond has the same topology for all amino acids except for proline. Thus, to derive a complete parameter set for the present purposes, ferrocene-1-(L)proline-1'-(L)alanine (Figure 2) was chosen for the parameterization of ferrocene-bearing peptides as this compound contains both proline and non-proline connections to ferrocene.

Parameters for ferrocene-1-(L)proline-1'-(L)alanine were developed by using a two-step procedure. First, the charges on ferrocene were calculated on the QM-optimized structure as described in the "Computational Methods" section above. The AFMM method was then used to obtain a complete set of parameters. The resulting  $\nu_j^{\max}$  versus  $\nu_i$  plot is shown in Figure 3. The corresponding value of  $\sigma = 77.2 \text{ cm}^{-1}$  is within the range of previous benchmark studies.<sup>[63,67]</sup>

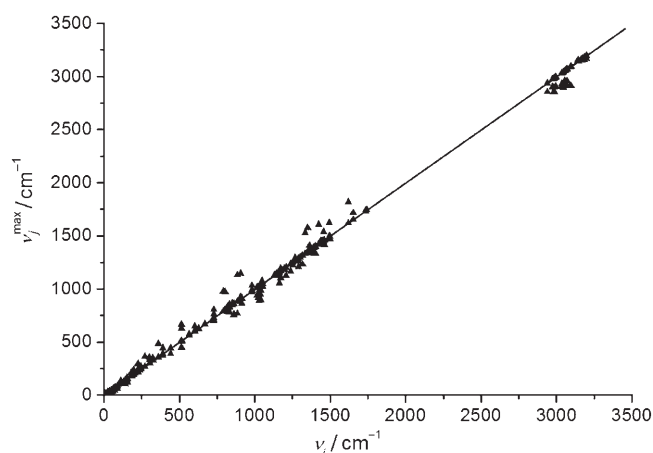


Figure 3. Frequency-matching plot ( $\nu_j^{\max}$  vs.  $\nu_i$ ) for ferrocene-1-alanine-1'-proline. The line is the ideal case where  $\nu_j^{\max} = \nu_i$ , that is, of perfectly matched frequencies and eigenvector projections. Symbols refer to optimized parameters.  $\sigma = 77.2 \text{ cm}^{-1}$ .

Atom type assignments and atomic partial charges, as well as the parameters obtained from AFMM, are listed in the Supporting Information section.

#### Parameterization of dichloromethane and creation of a solvent box:

Dichloromethane is one of the most widely used solvents for ferrocene-peptide chemistry. It was therefore useful to perform simulations in this solvent, in order to mimic the experimental conditions. Unfortunately, no all-atom parameters for dichloromethane exist in CHARMM, but similar solvents such as chloroform have already been successfully implemented in CHARMM within the united-atom approximation.<sup>[82]</sup> Here, the van der Waals parameters for chlorine were taken from the literature,<sup>[82]</sup> and for carbon and hydrogen other existing CHARMM van der Waals parameters were used. The AFMM method was then used to obtain a complete set of parameters. The resulting  $\nu_j^{\max}$  versus  $\nu_i$  plot, shown in Figure 4, corresponds to a value of  $\sigma = 37.6 \text{ cm}^{-1}$ .

#### Evaluation of the parameters

*Fc-(D-Ala-D-Pro-OEt)<sub>2</sub> crystal simulation:* Final evaluation of the parameter set should be performed against independent data. The present force field was tested on the available crystal structure of *Fc-(D-Ala-D-Pro-OEt)<sub>2</sub>*, a ferrocene-peptide derivative.<sup>[27]</sup> *Fc-(D-Ala-D-Pro-OEt)<sub>2</sub>* crystallizes in a tetragonal, *I*-centered lattice with group symmetry *I4<sub>1</sub>* and four molecules in the unit cell. MD calculations were performed for the whole crystal using periodic boundary conditions. The crystal was constrained to tetragonality (i.e.,  $\alpha = \beta = \gamma = 90^\circ$ ), but the unit cell dimensions were allowed to vary during both the energy minimization and the MD calculation. The energy minimized and the experimental cell vectors are reported in Table 1 as well as their average values after 0.1  $\mu\text{s}$  MD. The crystal lattice parameters are conserved over the simulation. After minimization, the cell

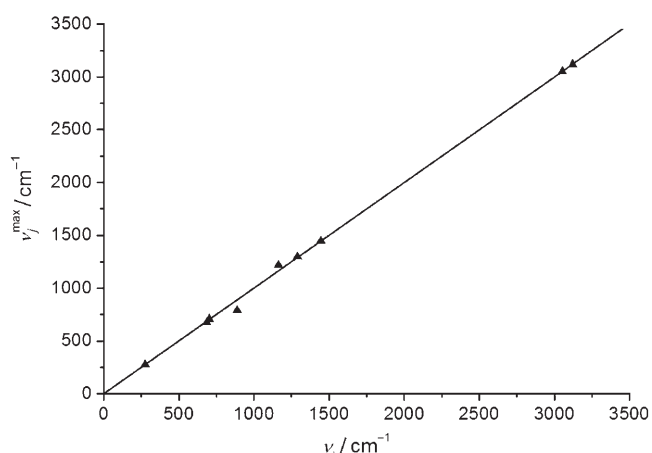


Figure 4. Frequency-matching plot ( $\nu_j^{\max}$  vs.  $\nu_i$ ) for dichloromethane. The line is the ideal case in which  $\nu_j^{\max} = \nu_i$ , that is, of perfectly matched frequencies and eigenvector projections. Symbols refer to optimized parameters.  $\sigma = 37.6 \text{ cm}^{-1}$ .

Table 1. Unit cell dimensions [ $\text{\AA}$ ] of *Fc-(D-Ala-D-Pro-OEt)<sub>2</sub>* crystal structure.

	Experimental	Minimized <sup>[a]</sup>	Dynamics <sup>[b]</sup>
<i>a</i>	14.573(2)	14.466	14.8(1)
<i>b</i>	14.573(2)	14.466	14.8(1)
<i>c</i>	14.953(2)	15.176	15.2(2)

[a] Minimized crystal unit cell after 10000 SD steps followed by 10000 ABNR minimization steps. [b] Mean values calculated over 0.1  $\mu\text{s}$  molecules dynamics at 298 K using the new CHARMM force field. Standard deviation in parentheses.

volume was computed to be  $3175.9 \text{ \AA}^3$ , within error and almost identical to the experimental value of  $3175.6 \text{ \AA}^3$ .

Ferrocene-bearing dipeptides are known to adopt a chiral organization in the solid state through hydrogen-bonds that connect both peptide strands.<sup>[29]</sup> Two kinds of intramolecular hydrogen-bond patterns have been experimentally observed (Figure 5): the ‘‘Herrick’’ conformation,<sup>[7]</sup> in which two hydrogen bonds connect both strands and the ‘‘van Staveren’’ conformation,<sup>[32]</sup> in which only one hydrogen bond connects the peptide strands. When both substituents point away from each other, no intramolecular hydrogen bonds are ob-

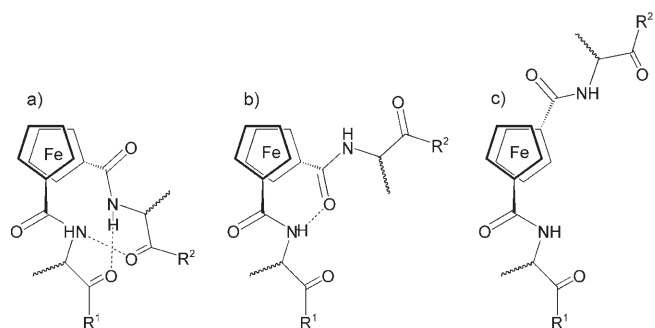


Figure 5. Representative scheme of different hydrogen-bonding patterns connecting two peptide strands attached to a ferrocene moiety a) Herrick, b) van Staveren, and c) open conformation.

served and this was coined as the “open” class of conformations.<sup>[29]</sup>

The experimentally-observed hydrogen-bond pattern in the  $\text{Fc}-(\text{D-Ala-D-Pro-OEt})_2$  crystal is of the Herrick type, as shown in Figure 5a. This pattern contains two  $C_2$ -symmetrical intramolecular hydrogen bonds between each alanine CO and the NH of the alanine of the other dipeptide chain.

To examine the stability of the intramolecular hydrogen-bond patterns, the distances between the hydrogen-bonded heavy atoms ( $\text{O}\cdots\text{N}$  distance) were monitored as a time series (Figure 6). The MD hydrogen bonds are slightly

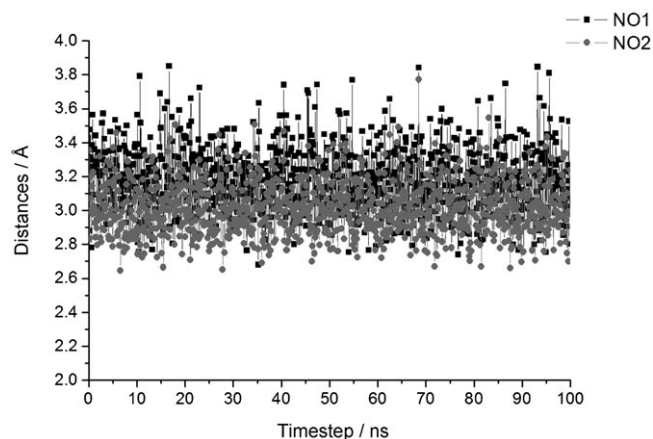


Figure 6. Time series of  $d_1(\text{N-O})$  (here NO1), in which N is the nitrogen of the first amide bond of one peptide strand and O the carbonyl oxygen of the second amide bond of the other. For  $d_2(\text{N-O})$  (here NO2) distances N is the corresponding nitrogen of the second peptide and O the carbonyl oxygen of the first peptide strand.

longer (0.2 Å on average) than those reported experimentally. However, the hydrogen-bonding pattern remains stable throughout the 100 ns simulation.

Another interesting feature of this crystal is that the ferrocene moieties are packed in a helically ordered arrangement with one turn equivalent to a 14.47 Å pitch height (see Figure 7), within which the distance between the closest ferrocene unit is 4.46 Å. The mean value of the pitch height arising from the MD calculation is  $14.24 \pm 0.15$  Å, within 5% of the experimentally measured value. A further feature of the crystal is that the ferrocene adopts a herringbone motif arrangement, in which the proline and the ethyl ester moieties individually form columns (Figure 7). The dipeptide chains (-Ala-Pro-OEt) induce this molecular aggregation through stacking of the intramolecular hydrogen-bond sites formed between the two alanines together with stacking of the hydrophobic proline rings. In this way, both the hydrophilic and the hydrophobic parts of the molecule stack to form the columns of the herringbone motif. The herringbone motif was found to be preserved throughout the 100 ns MD simulation. Both the proline and ethyl ester moieties remain stacked during the dynamics.

As shown in Figure 7, the minimized and experimental structures are very similar. The root-mean-square deviation

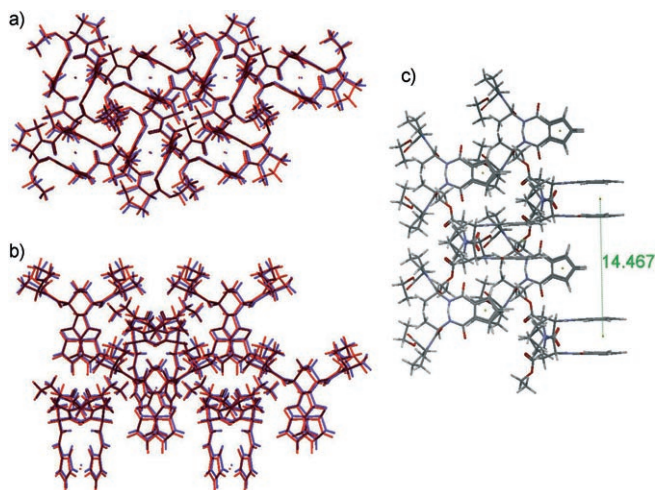


Figure 7. a) and b) superposition of one and a half unit cell of the minimized and experimental structures of  $\text{Fc}-(\text{D-Ala-D-Pro-OEt})_2$ <sup>[56]</sup> seen along the  $b$  and the  $c$  axes, respectively. c) Crystal seen along the  $a$  axis shows the pitch height.

(RMSD) arising from the heavy atoms for all four molecules of the unit cell, was found to be 1.35 Å. The side chains atoms and the C termini are more flexible than the backbone atoms, as evidenced by the crystallographic temperature factors, which are 10 to 15 Å<sup>2</sup> in the side chain compared to 2 to 9 Å<sup>2</sup> for the backbone atoms. The RMSD between the calculated and experimental backbone atoms of a single molecule in the crystal lattice was 0.32 Å.

*Fc-(D-Ala-D-Pro-OEt)2* and *Fc-(L-Ala-L-Pro-OEt)* in vacuum and in dichloromethane: MD simulations of  $\text{Fc}-(\text{D-Ala-D-Pro-OEt})_2$  and its enantiomer  $\text{Fc}-(\text{L-Ala-L-Pro-OEt})_2$  were performed in vacuum and in explicit dichloromethane. As these two structures are enantiomers all the results were found to be equivalent for the two structures. Therefore, for simplicity, only the results for the *D* conformation are shown.

As shown in Figure 8, the superposition of minimized and experimental structures is very close. The RMSD of the pep-

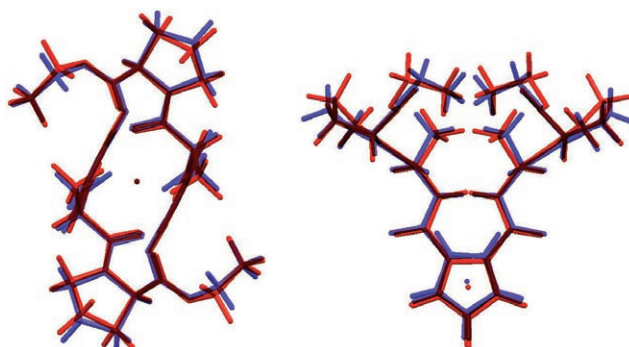


Figure 8. Superimposed minimized single molecule and crystal structure of ferrocene-1,[(D)alanine-(D)proline]-1',[(D)alanine-(D)proline],<sup>[83]</sup> along the  $a$  (left image) and  $c$  axis (right image) respectively. Similar results were obtained for the *L* enantiomers.

tion, the maximal deviation of 1.4 Å is lower than the 2.0 Å observed in vacuum, which seems to indicate that solvent molecules have a stabilizing effect on the intramolecular hydrogen bonding of the molecule.

tion, the maximal deviation of 1.4 Å is lower than the 2.0 Å observed in vacuum, which seems to indicate that solvent molecules have a stabilizing effect on the intramolecular hydrogen bonding of the molecule.

Table 2. Geometrical features of hydrogen-bond pattern for Fc-Ala-Pro.<sup>[a]</sup>

	$d_1(\text{HO})$ [Å]	$d_2(\text{HO})$ [Å]	$d_1(\text{NO})$ [Å]	$d_2(\text{NO})$ [Å]	$a_1(\text{NHO})$ [°]	$a_2(\text{NHO})$ [°]
exptl. <sup>[b]</sup>	2.053	2.053	2.98(1)	2.98(1)	146(5)	146(5)
crystal <sup>[c]</sup>	2.2(2)	2.0(2)	3.2(2)	3.0(2)	158(10)	162(9)
vacuum <sup>[d]</sup>	2.1(2)	2.1(2)	3.0(2)	3.0(2)	153(11)	153(11)
solvent <sup>[e]</sup>	2.05(2)	2.06(2)	3.0(2)	3.0(2)	155(10)	155(11)

[a]  $d_1$  and  $a_1$  represent the distance and the angle of the first hydrogen bond, respectively, and  $d_2$  and  $a_2$  are the distance and the angle of the second hydrogen bond, respectively; standard deviation is given in parentheses. [b] Average distances and angles measured on the crystal structure.<sup>[83]</sup> [c] Average distances and angles monitored in the crystalline state over the simulation time. [d] As a single molecule in a vacuum. [e] As a single molecule in dichloromethane.

the  $C_2$ -symmetrical intramolecular hydrogen-bonding network to within 2% of the experimentally observed distances. The hydrogen-bond pattern thus remains stable over the simulation and is not significantly affected by the absence of the crystal environment.

In general, ferrocene-peptide derivatives are soluble in low polarity solvents, such as dichloromethane, and structural studies are frequently carried out in this solvent. In order to reproduce as closely as possible the experimental condition, simulations were performed in explicit solvent. Minimized structures of Fc-(Ala-Pro-OEt)<sub>2</sub> are shown in Figure 9. The hydrogen bonds between both strands are pre-

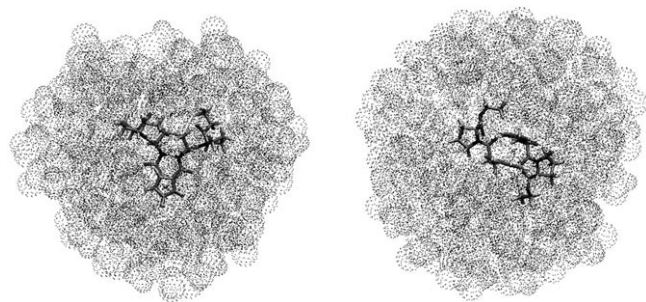


Figure 9. Top and side view of Fc-(Ala-Pro-OEt)<sub>2</sub> in a dichloromethane sphere (depicted as grey clouds) after minimization.

served in the explicit solvent simulations, as already observed in the vacuum simulation. The mean value of the hydrogen-bond length (defined as the NO distances) of  $3.01 \pm 0.20$  Å, measured during simulation in solution, is comparable to the  $3.00 \pm 0.17$  Å measured in vacuum for the time series (see Supporting Information). The results also match the bond lengths observed in the experimental X-ray single-crystal structure, which is  $2.98 \pm 0.10$  Å. However, in solu-

tion, the maximal deviation of 1.4 Å is lower than the 2.0 Å observed in vacuum, which seems to indicate that solvent molecules have a stabilizing effect on the intramolecular hydrogen bonding of the molecule.

The present results are in good agreement with the experimental solid-state structure observed in the crystal, and also with liquid-phase NMR and circular dichroism experiments. In the <sup>1</sup>H NMR spectrum of Fc-(Ala-Pro)<sub>2</sub> in CDCl<sub>3</sub> only one kind of N-H resonance was detected at low field (8.96 ppm; the two hydrogen bonds are equivalent because of the plane of symmetry),<sup>[84]</sup> and circular dichroism experiments also support the formation of a Herrick-type hydrogen-bond pattern. Thus, the two identical intramolecular hydrogen bonds between the dipeptide chains, observed during the simulations, are also observed in solid-state and solution-phase experimental studies.

**Hydrogenase mimics studied in vacuum and in solution:** The structural and dynamical features of potential synthetic models of the hydrogenase active site are now explored with MD, using the developed force field. Models 3–9 were investigated as potential chelating ligands for a nickel atom.

**Compound 3:** Structural and geometrical features of model 3 are shown in Figure 10 and Table 3. It was found experimentally that two diastereomers of compound 3 co-crystal-

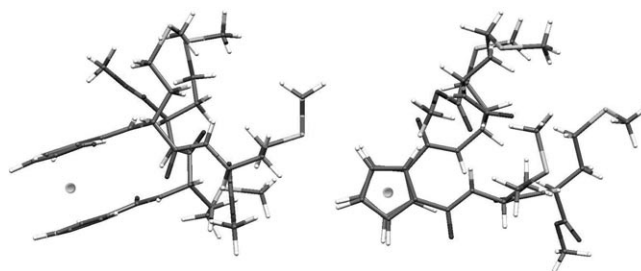


Figure 10. Top (left) and side (right) views of the energy minimized structure of ferrocene-1-[(D)methionine-(L)methionine]-1'-[(D)-methionine-(L)methionine].

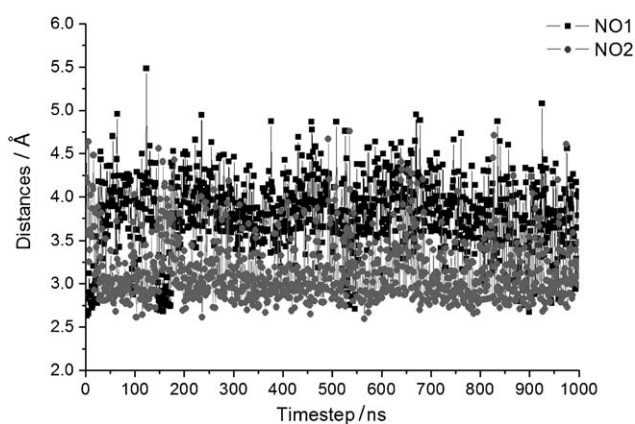
lized (ca. 20% (Met-L-Met-L)-Fc-(D-Met-L-Met) and 80% Fc-(D-Met-L-Met)<sub>2</sub>).<sup>[85]</sup> The X-ray structure observed is thus a weighted average between these diastereomers. As 80% of the conformers in the crystal were found in the ferrocene-1-[(D)methionine-(L)methionine]-1'-[(D)-methionine-(L)methionine] enantiomeric state, this molecule was chosen for a vacuum MD simulation. The backbone RMSD between the average structure of the isolated molecule and the experimental structure was found to be 1.2 Å.

During the heating process of the simulation, the first hydrogen bond was found to be relatively unstable deviating by up to 1 Å from its starting position (see Figure 11 and Table 3). However, the other geometrical properties of the hydrogen bonds shown in Table 3 are in good agreement with experimental results.

Table 3. Hydrogen bond experimental versus calculated geometrical properties for compound **3**.<sup>[a]</sup>

	$d_1(\text{HO})$ [Å]	$d_2(\text{HO})$ [Å]	$d_1(\text{NO})$ [Å]	$d_2(\text{NO})$ [Å]	$a_1(\text{NHO})$ [°]	$a_2(\text{NHO})$ [°]
exptl <sup>[b]</sup>	2.152	2.017	2.992	2.913	137.8	159.6
energy min <sup>[c]</sup>	2.029	1.896	2.862	2.889	138.8	172.2
MD <sup>[d]</sup>	3.3(5)	2.3(4)	3.8(4)	3.1(4)	128(3)	144(13)

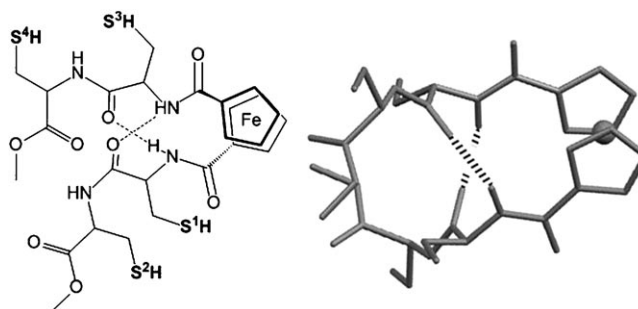
[a]  $d_1$  and  $a_1$  represent the distance and the angle of the first hydrogen bond, respectively, and  $d_2$  and  $a_2$  are the distance and the angle of the second hydrogen bond, respectively; standard deviation is given in parentheses. [b] Bond lengths and angles from the X-ray single-crystal structure.<sup>[85]</sup> [c] Energy-minimized bond lengths and angles measured after the minimization in vacuum. [d] Bond lengths and angles measured from the MD simulation in dichloromethane.  $d_1$  and  $a_1$  represent respectively the distance and the angle of the first hydrogen bond and  $d_2$  and  $a_2$  are the distance and the angle of the second hydrogen bond. Standard deviations are given in parentheses.

Figure 11. Time series of ferrocene-1-((D)methionine-(L)methionine)-1'-((D)methionine-(L)methionine) intramolecular hydrogen bonds over 1  $\mu\text{s}$  MD simulation in vacuum.

**Model systems 4, 5, 6, and 7:** Structural features of compounds **2–4** and model systems **5–7** that describe the ferrocene were examined. The distance between the Cp-ring carbon atoms and the iron atom, dihedral angles in the cyclopentadienyl ring, as well as geometrical features of the

hydrogen bonds between both peptide stands (bond length, angles, and dihedral angles of the hydrogen bonds) are listed in Table 4. In all instances both Cp rings remained parallel and the first amide bond attached to the ferrocene remains coplanar with the Cp ring.

Compound **4** forms two intramolecular hydrogen bonds, while model **5** forms just one, the only difference between these two compounds being the nickel atom chelated by the sulfur atoms in model **5**. A similar difference is observed between models **6** and **7**, as model **6** forms one intramolecular hydrogen bond when model **7**, with nickel incorporated, has none. Thus, the formation of a chelating pocket for nickel hinders the formation of a hydrogen bond between the two strands (see Table 4), and this was observed for both the simulation in vacuum and in explicit solvent. If model **4** adopted the open conformation, the chelation of a metal between the strands would be synthetically hindered. Compound **4** was subsequently synthesized, but has not yet been crystallized. The simulation of compound **4** shows that, both in vacuum and in solution, two Herrick-type hydrogen bonds form (Figure 12, right). The structure of compound **4**

Figure 12. Left: Representative scheme of “Herrick” hydrogen-bond pattern of  $\text{Fe}-(\text{L-Cys}(\text{SH}))- \text{L-Cys}(\text{SH})_2$ . Right: Model **4** after energy minimization.

was investigated in solution by NMR and CD spectroscopy (Figure 13). The highly symmetrical spectrum and a downfield-shifted signal for one amide proton ( $\delta=8.22$  ppm) is typical for the Herrick-type hydrogen bond. Furthermore,

Table 4. Summary of geometrical data calculated for the different model systems over 1  $\mu\text{s}$  molecular dynamics simulation in vacuum and 0.5  $\mu\text{s}$  in solution.<sup>[a]</sup>

	$\text{C}_{\text{Cp}}\text{Fe}$	$d_1(\text{HO})$ [Å]	$d_2(\text{HO})$ [Å]	$a_1(\text{NHO})$ [°]	$a_2(\text{NHO})$ [°]	$a(\text{OCN})$ [°]	$t(\text{C}_{\text{Cp}}\text{C}_{\text{Cp}}\text{C}_{\text{Cp}}\text{C}_{\text{Cp}})$ [°]	$t(\text{C}_{\text{Cp}}\text{C}_{\text{Cp}}\text{CN})$ [°]
<b>2</b>	2.06 (3)	2.1 (2)	2.1 (2)	153(11)	153(11)	119(3)	0(3)	3(5)
<b>2</b> <sup>[b]</sup>	2.08 (1)	2.05 (2)	2.06 (2)	155(10)	155(11)	119(3)	0(2)	2(15)
<b>2</b> <sup>[c]</sup>	2.06	2.05	2.05	145.5	145.5	119	0	5
<b>3</b>	2.07 (2)	2.20 (5)	X <sup>[d]</sup>	114(11)	X <sup>[d]</sup>	118(3)	0(2)	7(5)
<b>3</b> <sup>[b]</sup>	2.06	2.02	X <sup>[d]</sup>	138.2	X <sup>[d]</sup>	122	0	1
<b>4</b>	2.07 (2)	2.10 (3)	2.10 (3)	149(12)	149(12)	119(3)	0(2)	1(3)
<b>4</b> <sup>[b]</sup>	2.07 (1)	2.06 (3)	2.05 (2)	151(11)	151(11)	119(3)	0(2)	4(7)
<b>5</b>	2.08 (2)	2.20 (20)	X <sup>[d]</sup>	150(11)	X <sup>[d]</sup>	119(4)	0(2)	6(6)
<b>6</b>	2.05 (2)	2.40 (30)	X <sup>[d]</sup>	134(14)	X <sup>[d]</sup>	122(3)	0(2)	7(6)
<b>7</b>	2.10 (2)	X <sup>[d]</sup>	X <sup>[d]</sup>	X <sup>[d]</sup>	X <sup>[d]</sup>	119(3)	1(3)	7(5)

[a]  $\text{C}_{\text{Cp}}$  are cyclopentadienyl carbon atoms. C, N, H, and O belong to the first amide bond connected to the ferrocene.  $d$  represents the bond lengths,  $a$  the angles, and  $t$  the dihedral angles; standard deviations are given in parentheses. [b] Calculated from the simulation in explicit dichloromethane. [c] Based on the experimental X-Ray data.<sup>[83]</sup> [d] No hydrogen bond observed.

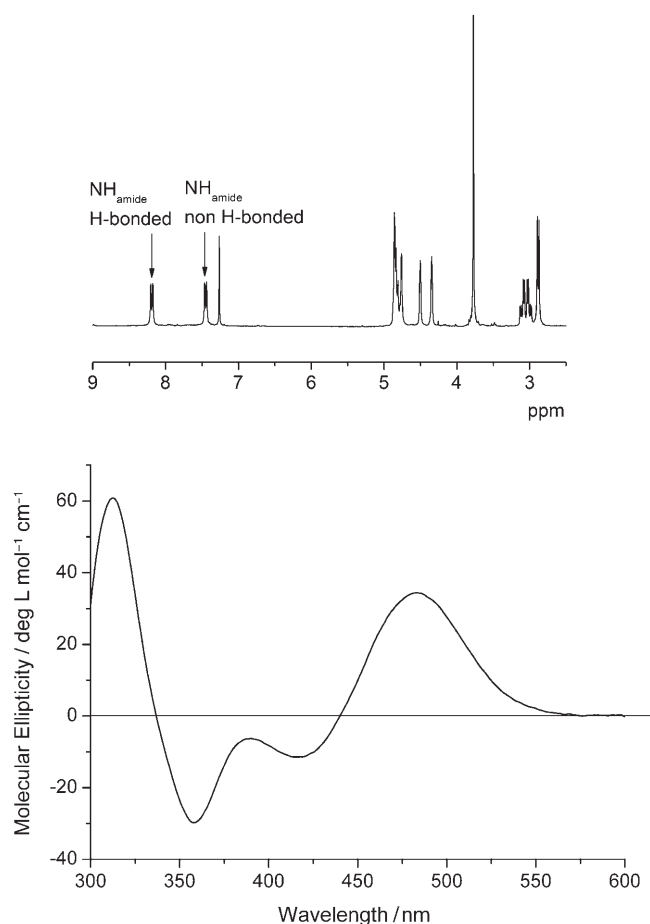


Figure 13. Top: <sup>1</sup>H NMR spectrum (400 MHz) of synthesized Fc(L-Cys(SH)-L-Cys(SH))<sub>2</sub> (model **4**); chloroform residual peak at 7.25 ppm. Bottom: Experimental CD spectrum of Fc(L-Cys(SH)-L-Cys(SH))<sub>2</sub> measured in CH<sub>2</sub>Cl<sub>2</sub>.

the CD spectrum shown in Figure 13 (bottom) exhibits a positive Cotton effect around 485 nm, characteristic of a Herrick-type hydrogen-bond pattern between the peptide strands and a P-helical geometry of the ferrocene.<sup>[29]</sup> Therefore, both the experimental data and the simulations are consistent with a Herrick conformation of compound **4** in solution.

The distances between the sulfur atoms were calculated from the simulations of **4** and **6** in vacuum and **4** in explicit CH<sub>2</sub>Cl<sub>2</sub> in order to examine the influence of the length of the peptide strands on the shape and the flexibility of the sulfur chelating shell. The results are shown in Table 5. The distances between the sulfur atoms are in the same range for both models. This is rather unexpected because the different length of the peptide strands in models **4** and **6** (2-mer versus 6-mer) suggested different thermal motions and therefore different atomic distance between the sulfur atoms.

The distances between any two sulfur atoms in the experimental crystal structure of the active site of [NiFe]-hydrogenase are 4.5–6 Å,<sup>[86]</sup> whereas the range observed during our MD simulations is 3.5–15 Å. That indicates that, for com-

Table 5. Average sulfur–sulfur distances for **4** and **6** in vacuum and for **4** in solution.<sup>[a]</sup>

	S <sup>1</sup> –S <sup>2</sup> [Å]	S <sup>1</sup> –S <sup>3</sup> [Å]	S <sup>1</sup> –S <sup>4</sup> [Å]	S <sup>2</sup> –S <sup>3</sup> [Å]	S <sup>2</sup> –S <sup>4</sup> [Å]	S <sup>3</sup> –S <sup>4</sup> [Å]
<b>4</b>	6.7(9)	7.0(9)	8.0(9)	8.2(10)	12.1(9)	6.1(11)
<b>4</b> <sup>[b]</sup>	5.9(1)	7.3(7)	8.1(8)	8.0(8)	11.8(9)	6.2(1)
<b>6</b>	12.7(6)	8.0(5)	12.7(9)	7.9(6)	6.1(10)	6.7(7)

[a] The numbering of sulfur atom refers to the numbering presented in Figure 12; standard deviations are given in parentheses. [b] Measured during simulation in explicit dichloromethane.

pound **4**, thermal energy alone is high enough to bring two sulfur atoms as close as 4 Å during the MD and therefore close enough to bind a nickel atom. The coordination of nickel seems thus feasible from a geometrical point of view. The next step was to include a nickel atom in the ligand pocket of **4** and **6**, so as to obtain models **5** and **7**. The nickel atom was included by using a harmonic bond energy term between the sulfur atoms and nickel. Simulation in vacuum was performed on molecules **4–7** following the protocol described in the “Computational Methods” section. The resulting minimized structures are shown in Figure 14.

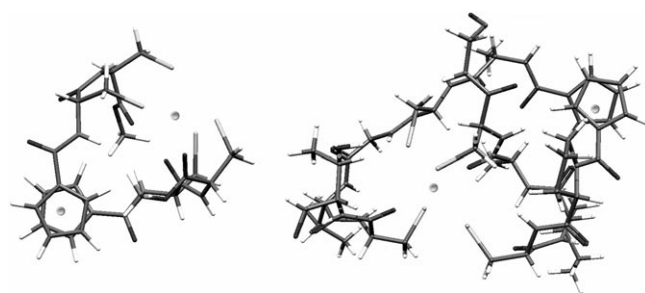


Figure 14. Structures of model **5** (left) and model **7** (right) after 1 μs MD in vacuum.

Mean values for the Ni–S atomic distances and S–Ni–S angles are reported over 1 μs MD in Table 6.

For model systems **5** and **7**, there was no apparent distortion of the peptides during the simulation. Steric hindrance

Table 6. Comparison between models **5**, **7**, and **9** and experimental values of Ni–S distances and S–Ni–S angles.<sup>[a]</sup>

	S <sup>1</sup> –Ni [Å]	S <sup>2</sup> –Ni [Å]	S <sup>3</sup> –Ni [Å]	S <sup>4</sup> –Ni [Å]	S <sup>1</sup> –Ni–S <sup>2</sup> [°]	S <sup>1</sup> –Ni–S <sup>3</sup> [°]	S <sup>1</sup> –Ni–S <sup>4</sup> [°]
exptl <sup>[b]</sup>	2.51	2.37	2.49	2.48	93.3	181.8	74.6
<b>5</b>	2.31(5)	2.25(4)	2.30(5)	2.27(6)	96(4)	160(5)	94(4)
<b>7</b>	2.33(6)	2.29(5)	2.28(5)	2.28(5)	90(3)	173(3)	89(3)
<b>9</b>	2.33(7)	2.32(7)	2.34(7)	2.37(0.8)	96(4)	95(4)	95(8)

[a] See structure diagrams for sulfur numbering; standard deviations are given in parentheses. [b] Experimental values measured on the Hydrogenase active site were obtained from the Protein Data Bank (PDB entry 1FRV).

due to coordination of the nickel in the sulfur ligand pocket is therefore not a problem. Nickel–sulfur complexes con-

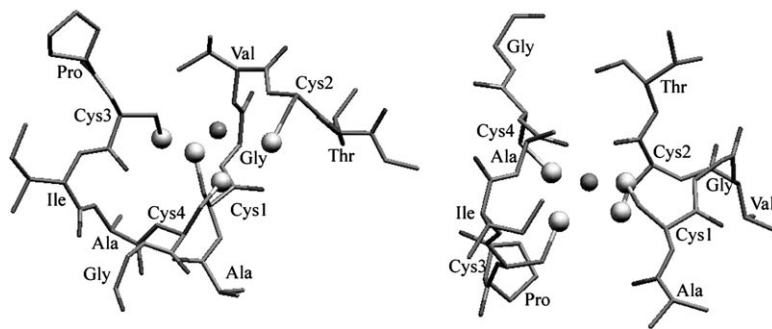


Figure 15. Model **9** (left) energy-minimized structure versus (left) X-ray experimental structure (structure of the active site obtained from the PDB, ref: 1FRV).

nected to an aliphatic carbon chain are comparatively rare in the literature; less than 30 crystal structures have been published as revealed by a CSD database search. In the present simulation the S–Ni bonds are in the range of 2.25 Å to 3.0 Å (see Table 6), similar to those in the crystal structures of [NiFe]-hydrogenase,<sup>[72]</sup> which are in the range of 2.37 Å to 2.51 Å. These results are also in good geometrical agreement with DFT/B3LYP optimizations performed on various nickel complexes.<sup>[87]</sup>

*Simulation of mimics of the hydrogenase active center (model systems **8** and **9**):* Model systems **8** and **9** are models of the enzyme active site, and do not contain ferrocene. They were simulated using the standard CHARMM22 force field,<sup>[45]</sup> except for the nickel atom, which was modeled as described in the “Computational Methods” section. The sequence that surrounds the metal core in the natural enzyme active site is: -NH-Ala-Cys<sup>1</sup>-Gly-Val-Cys<sup>2</sup>-Thr-CO- and -NH-Pro-Cys<sup>3</sup>-Ile-Ala-Cys<sup>4</sup>-Gly-CO- (see Figure 15). An MD simulation of these two systems in vacuum was performed for 500 ns.

In model **8**, Cys<sup>1</sup> is connected to Cys<sup>4</sup> and Cys<sup>2</sup> to Cys<sup>3</sup> via two disulfide bridges. In model **9**, a nickel atom is incorporated between the sulfur atoms and bridges the cysteine residues on opposite peptide chains (Figure 15). In the latter case, it was found that no additional harmonic restraint was needed for holding the nickel atom in the sulfur ligand pocket; electrostatic and nonbonded interactions were sufficient to hold the structure together over the length of the MD run.

The distances between the termini of the two strands over the 500 ns dynamics run at room temperature were monitored for systems **8** and **9** (Table 7). In both cases, the mean distance between both N termini (about 9–12 Å) is larger than the mean distance between the C termini (5–10 Å). Since the distance between the two cyclopentadienyl rings in ferrocene is about 3.3 Å, this may indicate that ferrocene could be attached more easily to the C termini than the N termini. The N<sub>ter</sub>–C<sub>ter</sub> distances are also in the range of 3–5 Å. Therefore, binding of ferrocene to both N termini of the peptides seems the least favorable option. A parallel orientation of the peptide strands, but with ferrocene connect-

ing the C termini, seems sterically more promising. Alternatively, an antiparallel orientation of the peptides with the C terminus of one strand and the N terminus of the other strand attached to the ferrocene may also be possible. Using 1'-aminoferrocene-1-carboxylic acid as the ferrocene template, such antiparallel oriented peptides were already synthesized in our group and their structures in-

Table 7. Average distances measured between the C and the N termini of model systems **8** and **9**, and of the *Desulfovibrio Gigas* hydrogenase experimental crystal structure.<sup>[a]</sup>

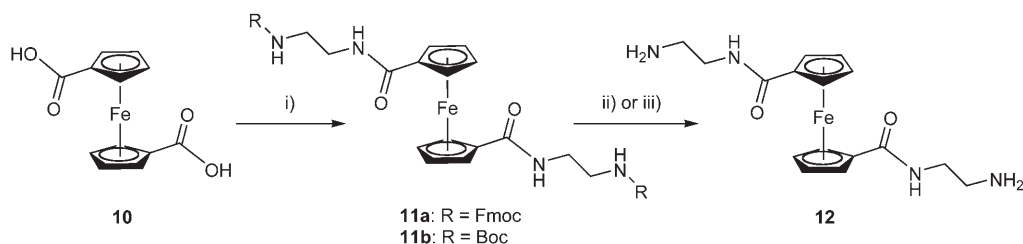
	C <sub>ter</sub> <sup>1</sup> –C <sub>ter</sub> <sup>2</sup> [Å]	N <sub>ter</sub> <sup>1</sup> –C <sub>ter</sub> <sup>1</sup> [Å]	N <sub>ter</sub> <sup>1</sup> –C <sub>ter</sub> <sup>2</sup> [Å]	N <sub>ter</sub> <sup>1</sup> –N <sub>ter</sub> <sup>2</sup> [Å]	N <sub>ter</sub> <sup>2</sup> –C <sub>ter</sub> <sup>1</sup> [Å]	N <sub>ter</sub> <sup>2</sup> –C <sub>ter</sub> <sup>2</sup> [Å]
<b>8</b>	5.3(2)	5.3(7)	6.6(3)	9.6(8)	8.1(11)	5.1(7)
<b>9</b>	10.0(0.58)	10.4(1.48)	6.5(2.61)	12.19(1.80)	6.25(1.31)	14.2(1.45)
exptl <sup>[b]</sup>	15.24	8.75	9.99	15.82	15.49	11.26

[a] C<sub>ter</sub><sup>1</sup> belongs to the threonine on the first strand; C<sub>ter</sub><sup>2</sup> belongs to the glycine of the second sequence. N<sub>ter</sub><sup>1</sup> is attached to the alanine of the first strand and N<sub>ter</sub><sup>2</sup> to the proline of the second one; standard deviations are given in parentheses [b] Values measured for the experimental crystal structure of [NiFe]-hydrogenase of *Desulfovibrio Gigas* (PDB entry 1FRV).

investigated.<sup>[38,88]</sup> In the next section we describe the synthesis of a new ferrocene building block that could be used for the incorporation of ferrocene at the C termini of the peptides in a parallel orientation.

**Synthetic results:** Based on the simulation results, connecting ferrocene to C termini instead of the N termini of parallel peptide strands seemed preferable. The synthesis and application of 1,1'-diaminoferrocene in peptide synthesis has recently been reported.<sup>[89]</sup> One of the steps for the synthesis of 1,1'-diaminoferrocene is the formation of 1,1'-diazidoferrocene, which is temperature sensitive and potentially explosive. For this reason alone, 1,1'-diaminoferrocene does not seem to be a prudent choice for hydrogenase mimics. In addition, our calculations suggest that a higher degree of flexibility may be required. Starting from ferrocene-1,1'-dicarboxylic acid **10**, we decided to extend both Cp rings with an ethylenediamine spacer to arrive at compound **12** as the key starting material (Scheme 1). Three different synthetic approaches were tested by using Boc-protected ethylenediamine, Fmoc-protected or unprotected ethylenediamine. The protecting groups were removed as depicted in Scheme 1.

The Fmoc cleavage of compound **11a** occurs cleanly in solution.<sup>[90]</sup> However, workup requires chromatography on silica with careful control of the conditions. Cleavage of the Boc-protecting group of compound **11b** takes place in TFA with a large excess of phenol as an anti-oxidant. For the



Scheme 1. Synthesis of ferrocene ethylenediamine derivatives **12**. i) HOBt, DCC, DIEA, CH<sub>2</sub>Cl<sub>2</sub>, 1 h, 20 °C NH<sub>2</sub>-(CH<sub>2</sub>)<sub>2</sub>-NH-R, 4 h, 20 °C; ii) Piperidine/CH<sub>2</sub>Cl<sub>2</sub>, 30 min, 20 °C (for **11a**) or iii) TFA/Phenol 1 h, 20 °C (for **11b**).

third synthetic path using unprotected ethylenediamine, prior activation of ferrocene carboxylic acid and its isolation from the activation reagent is required, followed by addition of ethylenediamine. However, the reaction mixture has to be diluted to avoid polymerization. Even so, about 20% of the ferrocene–ethylenediamine macrocycle and/or polymers were formed which are difficult to removed from the desired product. Taking all aspects into account, there is a preference for the use of the Fmoc strategy, which is described in the Experimental Section. The ferrocene ethylenediamine **12** is now available as starting material for further coupling reactions with peptide derivatives.

## Conclusion

An all-atom CHARMM22 molecular mechanics force field has been developed and tested here for ferrocene-bearing peptides. Fitting the molecular mechanics potential to that derived by quantum chemical calculations produced a good matching of the normal modes of vibration for ferrocene-1-proline-1'-alanine. This molecule was used to derive the parameters for ferrocene and for the bonding between ferrocene and the first amide bond of the peptide sequence. Given the increasing importance of ferrocene peptide conjugates,<sup>[29,41–43]</sup> we believe that this force field will be of wide use.

The new parameters were subsequently applied to MD simulations of known compounds and the results obtained are in good overall agreement with the available experimental data in solution as well as in the solid state. Energy minimization and MD simulations of the Fc-(D-Ala-D-Pro)<sub>2</sub> crystal structure led to unit cell dimensions and volume being reproduced within less than 2% of the experimental values. Characteristic structural features of the solid state, such as the intramolecular hydrogen-bond pattern and the helical ferrocene arrangement are also accurately reproduced. Moreover, results obtained from the simulation in dichloromethane agree with NMR and CD spectroscopic investigations in solution.

The structure and dynamics of possible hydrogenase mimics were also examined here, both in vacuum and in explicit dichloromethane solvent. MD simulations of the model systems exhibited the formation of intramolecular hydrogen bonds between the two peptide strands of com-

pounds **2–6** that are consistent with the available experimental data. One surprising aspect is that small Cys–Cys dipeptides such as **4** will furnish a sulfur chelating shell very similar to that of longer peptides (**6**), which are based on the original hydrogenase sequences with a Cys–Aaa–Aaa–Cys motif. This is a highly encouraging result as the synthesis of dipeptides is a lot easier than that of any longer peptides and may still provide sufficiently accurate models.

Finally, two non-ferrocene hydrogenase mimics (model systems **8** and **9**) were studied. The mean distance between the C termini of the peptides during the MD was smaller than that of the N termini. This suggests that ferrocene attachment should be on the C termini of the peptides rather than on the N termini, as was the synthetic strategy hitherto followed. A novel synthetic strategy using a diamino–ferrocene derivative instead of ferrocene dicarboxylic acid is thus proposed and the synthesis of the required ferrocene template is described.

The present work represents a first step in the development of hydrogenase mimics of potential use in alternative energy production. The conformational complexity of the ferrocene peptide mimics requires the use of molecular simulation to prescreen plausible compounds for geometric suitability in chelating essential metals, prior to attempted synthesis. The present work demonstrates the development of a molecular mechanics force field for this purpose. Modeling and simulation were used to suggest new synthetic strategies. Future work will extend the integrated modeling/synthesis approach to design, synthesize and test further compounds incorporating key hydrogenase catalytic characteristics. To this end, ferrocene-derived cystein-containing peptides based on the design principles described herein are currently synthesized and their ability to form biomimetic metal complexes is being investigated in our laboratories.

## Experimental Section

CH<sub>2</sub>Cl<sub>2</sub> and *N,N'*-diisopropylethylamine (DIEA) were distilled over CaH<sub>2</sub> prior to use under inert atmosphere. MeOH, piperidine, CDCl<sub>3</sub>, CD<sub>3</sub>OD, distilled water, (all of them ACS grade) were used as purchased. All reactions were carried out under inert atmosphere of nitrogen or argon in dried glassware. (*9H*-Fluoren-9-yl)methyl-2-aminoethylcarbamate (EDA) and *O*-benzotriazol-1-yl-*N,N,N,N'*-tetramethyluronium tetrafluoroborate (TBTU) were obtained from Novabiochem and used without further purification. Ferrocene dicarboxylic acid was purchased

from Acros. Columns for column chromatography were packed with 0.063–0.200 mm silica gel 60 (VWR). Plastic coated with silica gel F<sub>254</sub> were used for TLC. NMR spectra were determined on a Bruker AM360 spectrometer, <sup>1</sup>H operating at 360.95 MHz and <sup>13</sup>C operating at 90.56 MHz. Peak positions in both the <sup>1</sup>H and the <sup>13</sup>C NMR spectra are reported in ppm relative to TMS, the internal standard. Spectra of peptides only are referenced to the residual MeOH signal (3.31 ppm <sup>1</sup>H, 49.0 ppm <sup>13</sup>C), or to the residual CHCl<sub>3</sub> signal (7.26 ppm <sup>1</sup>H, 77 ppm <sup>13</sup>C). Coupling constants, *J*, are reported in Hz. Individual peaks are marked as: singlet (s), doublet (d), triplet (t) or multiplet (m), or noted as pseudo signal (p). Elemental analysis was performed on a Foss Heraeus Vario EL Elemental Analysator in C,H,N mode. Mass spectra were measured on a Mat 8200 instrument, EI (70 eV) and FAB (glycerol or NBA matrix).

**Ferrocene-1-EDA-Fmoc-1'-EDA-Fmoc (11a):** A stirred suspension of ferrocene dicarboxylic acid (2.6 mmol; 719 mg) in freshly distilled and degassed CH<sub>2</sub>Cl<sub>2</sub> (50 mL) was placed under argon. Stoichiometric amounts of TBTU (5.2 mmol; ca. 1.67 g) and DIEA (2.5 mmol; ca. 1.0 mL) were added to this suspension. The resulting slurry was stirred at ambient temperature for 15 min (until entire dissolution). The reaction mixture was filtered to remove unreacted materials, and the residue was washed with freshly distilled and degassed CH<sub>2</sub>Cl<sub>2</sub>. The filtrate was then again placed under argon and cooled to 0°C. In parallel, another flask was charged with EDA (2.0 equiv, 5.2 mmol, ca. 1.12 g) and DIEA (2.5 equiv, ca. 1.0 mL) in CH<sub>2</sub>Cl<sub>2</sub> (20 mL). After 5 min at room temperature, this mixture was transferred to the other flask through a stainless steel canula by using standard Schlenk techniques. The reaction mixture was heated to room temperature and was subsequently stirred for 4 h at ambient temperature. The reaction mixture was then diluted with CH<sub>2</sub>Cl<sub>2</sub> (100 mL) and washed subsequently with distilled water (50 mL), saturated NaHCO<sub>3</sub> solution (50 mL), water (50 mL), 0.1 M HCl (50 mL), and distilled water (50 mL). The organic layer was then dried over MgSO<sub>4</sub>, filtered, and dried under reduced pressure to yield an orange solid (yield: 1.98 g, 95%); elemental analysis calcd (%) for C<sub>26</sub>H<sub>38</sub>FeN<sub>4</sub>O<sub>6</sub> (802.69): C 68.83, H 5.27, N 6.98; found: C 68.68, H 5.44, N 6.73; MS(FAB): *m/z*: 803.3 [M+H]<sup>+</sup>; <sup>1</sup>H NMR (CDCl<sub>3</sub>, 293 K, *c* = 10<sup>-2</sup> M): δ = 7.73 (pd, *J*<sub>app</sub> = 7.53 Hz, 4H; CH<sub>Fmoc</sub>), 7.57 (pd, *J*<sub>app</sub> = 7.66 Hz, 4H; CH<sub>Fmoc</sub>), 7.37 (pt, *J*<sub>app</sub> = 7.35 Hz, 4H; CH<sub>Fmoc</sub>), 7.24 (pt, *J*<sub>app</sub> = 7.23 Hz, 4H; CH<sub>Fmoc</sub>), 7.07 (brs, 1H; NH<sub>amide</sub>), 6.06 (brs, 1H; NH<sub>amide</sub>), 4.52 (brs, 4H; CH<sub>CP</sub>), 4.35–4.45 (m, 8H; CH<sub>CP</sub> + CH<sub>2,Fmoc</sub>), 4.18 (t, *J* = 4.2 Hz, 2H; CH<sub>Fmoc</sub>), 3.48 ppm (m, 8H, CH<sub>2,EDA</sub>).

**Ferrocene-1-EDA-NH<sub>2</sub>-1'-EDA-NH<sub>2</sub> (12):** Compound **11a** (0.7 mmol, ca. 570 mg) was dissolved in CH<sub>2</sub>Cl<sub>2</sub> (15 mL) and placed under argon. Piperidine (15 mL) was then added and the reaction mixture was stirred at ambient temperature until the reaction had reached completion (ca. 20 min). Solvents were then removed and residue was triturated with cold methanol and filtered to remove a white precipitate. The volume of the methanol was then reduced and the product was precipitated by the addition of cold CH<sub>2</sub>Cl<sub>2</sub>. After filtration, a brownish solid was obtained which decomposed rapidly in presence of air. The residue was then subjected to chromatography on silica gel (EtOAc/*n*-hexane 3:1) to yield an orange solid (yield: 185 mg, 74%); MS(EI): *m/z* calcd for C<sub>26</sub>H<sub>38</sub>FeN<sub>4</sub>O<sub>6</sub>: 358.11; found: 358.2 [M]<sup>+</sup>; <sup>1</sup>H NMR (CD<sub>3</sub>OD, 293 K, *c* = 10<sup>-2</sup> M): δ = 4.79 (pt, *J*<sub>app</sub> = 1.71 Hz, 4H; CH<sub>CP</sub>), 4.47 (pt, *J*<sub>app</sub> = 1.74 Hz, 4H; CH<sub>CP</sub>), 3.54 (t, *J* = 5.8 Hz, 4H; CH<sub>2,EDA</sub>), 3.08 ppm (dt, <sup>2</sup>*J* = 5.88 Hz, <sup>1</sup>*J* = 0.5 Hz, 4H; CH<sub>2,EDA</sub>).

## Acknowledgements

The authors are grateful to Drs. L. Meinhold, V. Kurkal-Siebert, M. Krishnan, and S. Fischer for many helpful discussions. Financial support from the Fond der Chemischen Industrie and the Deutsche Forschungsgemeinschaft (DFG, SFB 623) are gratefully acknowledged. The quantum mechanics calculations were performed on the HELICS, IWR-Universität Heidelberg (HFBG funds, hww cooperation). X.d.H. performed a cotutelle de thèse between the universities of Bordeaux and Heidel-

berg. Additional cotutelle support from the French Ministry of Research is also gratefully acknowledged.

- [1] N. Fey, *J. Chem. Technol. Biotechnol.* **1999**, *74*, 852.
- [2] R. Cammack, *Nature* **1999**, *397*, 214.
- [3] P. F. Weaver, S. Lien, M. Seibert, *Sol. Energy* **1980**, *24*, 3.
- [4] A. Volbeda, M. H. Charon, C. Piras, E. C. Hatchikian, M. Frey, J. C. Fontecilla-Camps, *Nature* **1995**, *373*, 580.
- [5] T. B. Rauchfuss *Inorg. Chem.* **2004**, *43*, 14.
- [6] I. P. Georgakaki, M. Y. Darensbourg, in *Comprehensive Coordination Chemistry II, Vol. 8* (Eds.: L. Que Jr., W. B. Tolman) Elsevier, Amsterdam, **2003**, p. 549.
- [7] D. J. Evans, C. J. Pickett, *Chem. Soc. Rev.* **2003**, *32*, 268.
- [8] A. C. Marr, D. J. E. Spencer, M. Schroder, *Coord. Chem. Rev.* **2001**, *219*, 1055.
- [9] M. Y. Darensbourg, E. J. Lyon, J. J. Smee, *Coord. Chem. Rev.* **2000**, *206–207*, 533.
- [10] J. C. Fontecilla-Camps, S. W. Ragsdale, *Adv. Inorg. Chem.* **1999**, *47*, 283.
- [11] M. Frey, *Struct. Bonding* **1998**, *90*, 97.
- [12] J. C. Fontecilla-Camps, A. Volbeda, M. Frey, *Trends Biotechnol.* **1996**, *14*, 417.
- [13] D. Chong, I. P. Georgakaki, R. Mejia-Rodriguez, J. Sanabria-Chinchilla, M. P. Soriaga, M. Y. Darensbourg, *Dalton Trans.* **2003**, 4158.
- [14] S. J. Borg, T. Behrsing, S. P. Best, M. Razavet, X. Liu, C. J. Pickett, *J. Am. Chem. Soc.* **2004**, *126*, 16988.
- [15] S. Ott, M. Borgström, M. Kritikos, R. Lomoth, J. Bergquist, B. Åkermark, L. Hammarström, L. Sun, *Inorg. Chem.* **2004**, *43*, 4683.
- [16] S. Ott, M. Kritikos, B. Åkermark, L. Sun, R. Lomoth, *Angew. Chem.* **2004**, *116*, 1024; *Angew. Chem. Int. Ed.* **2004**, *43*, 1006.
- [17] C. Tard, X. Liu, S. K. Ibrahim, M. Bruschi, L. De Gioia, S. C. Davies, X. Yang, L.-S. Wang, G. Sawers, C. J. Pickett, *Nature* **2005**, *433*, 610.
- [18] I. P. Georgakaki, L. M. Thomson, E. J. Lyon, M. B. Hall, M. Y. Darensbourg, *Coord. Chem. Rev.* **2003**, *238–239*, 255.
- [19] M. Stein, W. Lubitz, *J. Inorg. Biochem.* **2004**, *98*, 862.
- [20] M. Stein, W. Lubitz, *Phys. Chem. Chem. Phys.* **2001**, *3*, 2668.
- [21] M. Stein, E. van Lenthe, E. J. Baerends, W. Lubitz, *J. Am. Chem. Soc.* **2001**, *123*, 5839.
- [22] S. Niu, M. B. Hall, *Inorg. Chem.* **2001**, *40*, 6201.
- [23] H.-J. Fan, M. B. Hall, *J. Am. Chem. Soc.* **2001**, *123*, 3828.
- [24] R. M. Mege, C. Bourdillon, *J. Biol. Chem.* **1985**, *260*, 14701.
- [25] B. H. Huynh, D. S. Patil, I. Moura, M. Teixeira, J. J. Moura, D. V. DerVartanian, M. H. Czechowski, B. C. Prickril, H. D. Peck, Jr., J. LeGall, *J. Biol. Chem.* **1987**, *262*, 795.
- [26] R. S. Herrick, R. M. Jarret, T. P. Curran, D. R. Dragoli, M. B. Flaherty, S. E. Lindyberg, R. A. Slate, L. C. Thornton, *Tetrahedron Lett.* **1996**, *37*, 5289.
- [27] T. Moriuchi, A. Nomoto, K. Yoshida, A. Ogawa, T. Hirao, *J. Am. Chem. Soc.* **2001**, *123*, 68.
- [28] T. Moriuchi, T. Hirao, *Chem. Soc. Rev.* **2004**, *33*, 294.
- [29] S. I. Kirin, H.-B. Kraatz, N. Metzler-Nolte, *Chem. Soc. Rev.* **2006**, *35*, 348.
- [30] U. Hoffmanns, N. Metzler-Nolte, *Bioconjugate Chem.* **2006**, *17*, 204.
- [31] X. de Hatten, T. Weyhermueller, N. Metzler-Nolte, *J. Organomet. Chem.* **2004**, *689*, 4856.
- [32] D. R. van Staveren, T. Weyhermueller, N. Metzler-Nolte, *Dalton Trans.* **2003**, 210.
- [33] H.-B. Kraatz, J. Luszyk, G. D. Enright, *Inorg. Chem.* **1997**, *36*, 2400.
- [34] A. Nomoto, T. Moriuchi, S. Yamazaki, A. Ogawa, T. Hirao, *Chem. Commun.* **1998**, 1963.
- [35] T. Moriuchi, A. Nomoto, K. Yoshida, T. Hirao, *J. Organomet. Chem.* **1999**, *589*, 50.
- [36] K. Heinze, M. Schlenker, *Eur. J. Inorg. Chem.* **2004**, 2974.
- [37] K. Heinze, U. Wild, M. Beckmann, *Eur. J. Inorg. Chem.* **2007**, 617.
- [38] L. Barisic, M. Dropucic, V. Rapic, H. Pritzkow, S. I. Kirin, N. Metzler-Nolte, *Chem. Commun.* **2004**, 2004.

- [39] L. Barisic, M. Cakic, K. A. Mahmoud, Y.-n. Liu, H.-B. Kraatz, H. Pritzkow, S. I. Kirin, N. Metzler-Nolte, V. Ropic, *Chem. Eur. J.* **2006**, *12*, 4965.
- [40] L. Barisic, V. Ropic, N. Metzler-Nolte, *Eur. J. Inorg. Chem.* **2006**, 4019.
- [41] S. Chowdhury, D. A. R. Sanders, G. Schatte, H.-B. Kraatz, *Angew. Chem.* **2006**, *118*, 765; *Angew. Chem. Int. Ed.* **2006**, *45*, 751.
- [42] S. K. Dey, H.-B. Kraatz, *Bioconjugate Chem.* **2006**, *17*, 84.
- [43] F. Noor, A. Wüstholtz, R. Kinscherf, N. Metzler-Nolte, *Angew. Chem.* **2005**, *117*, 2481; *Angew. Chem. Int. Ed.* **2005**, *44*, 2429.
- [44] P. V. Bernhardt, P. Comba, *Inorg. Chem.* **1992**, *31*, 2638.
- [45] B. R. Brooks, R. E. Bruccoleri, B. D. Olafson, D. J. States, S. Swaminathan, M. Karplus, *J. Comput. Chem.* **1983**, *4*, 187.
- [46] B. Bosnich, *Chem. Soc. Rev.* **1994**, *23*, 387.
- [47] M. J. Sherrod, *Carbohydr. Res.* **1989**, *192*, 17.
- [48] Y.-D. Gao, K. B. Lipkowitz, F. A. Schultz, *J. Am. Chem. Soc.* **1995**, *117*, 11932.
- [49] G. Wilkinson, M. Rosenblum, M. C. Whiting, R. B. Woodward, *J. Am. Chem. Soc.* **1952**, *74*, 2125.
- [50] S. I. Kirin, U. Schatzschneider, X. De Hatten, T. Weyhermüller, N. Metzler-Nolte, *J. Organomet. Chem.* **2006**, *691*, 3451.
- [51] Insight II, Accelrys, **1998**.
- [52] A. D. MacKerell, Jr., D. Bashford, M. Bellott, R. L. Dunbrack, J. D. Evanseck, M. J. Field, S. Fischer, J. Gao, H. Guo, S. Ha, D. Joseph-McCarthy, L. Kuchnir, K. Kuczera, F. T. K. Lau, C. Mattos, S. Michnick, T. Ngo, D. T. Nguyen, B. Prodhom, W. E. Reiher, III, B. Roux, M. Schlenkrich, J. C. Smith, R. Stote, J. Straub, M. Watanabe, J. Wiorkiewicz-Kuczera, D. Yin, M. Karplus, *J. Phys. Chem. B* **1998**, *102*, 3586.
- [53] HBUILD, Polar Hydrogen Parameter Set for CHARMM Version 22 (Polar Hydrogens Only), Molecular Simulations, Inc., Waltham, MA (USA) **1992**.
- [54] NWChem 4.5, A Computational Chemistry Package for Parallel Computers, Pacific Northwest National Laboratory, Richland, Washington (USA), **2001**.
- [55] E. Bencze, J. Mink, C. Nemeth, W. A. Herrmann, B. V. Lokshin, F. E. Kuhn, *J. Organomet. Chem.* **2002**, *642*, 246.
- [56] M. Swart, J. G. Snijders, *Theor. Chem. Acc.* **2004**, *111*, 56.
- [57] S. Huzinaga, C. Arnau, *J. Chem. Phys.* **1970**, *53*, 451.
- [58] A. P. Scott, L. Radom, *J. Phys. Chem.* **1996**, *100*, 16502.
- [59] C. M. Breneman, K. B. Wiberg, *J. Comput. Chem.* **1990**, *11*, 361.
- [60] J. L. Lebowitz, J. K. Percus and L. Verlet, *Phys. Rev.* **1967**, *153*, 250.
- [61] R. Blom, A. Hammel, A. Haaland, J. Weidlein, T. V. Timofeeva, Y. T. Struchkov, *J. Organomet. Chem.* **1993**, *462*, 131.
- [62] T. N. Doman, C. R. Landis, B. Bosnich, *J. Am. Chem. Soc.* **1992**, *114*, 7264.
- [63] P. Comba, T. W. Hambley, *Molecular Modeling of Inorganic Compounds*, **2000**, p. 317.
- [64] A. C. Vaiana, Z. Cournia, I. B. Costescu, J. C. Smith, *Comput. Phys. Commun.* **2005**, *167*, 34.
- [65] A. C. Vaiana, H. Neuweiler, A. Schulz, J. Wolfrum, M. Sauer, J. C. Smith, *J. Am. Chem. Soc.* **2003**, *125*, 14564.
- [66] A. C. Vaiana, A. Schulz, J. Wolfrum, M. Sauer, J. C. Smith, *J. Comput. Chem.* **2003**, *24*, 632.
- [67] Z. Cournia, A. C. Vaiana, G. M. Ullmann, J. C. Smith, *Pure Appl. Chem.* **2004**, *76*, 189.
- [68] Z. Cournia, J. C. Smith, G. M. Ullmann, *J. Comput. Chem.* **2005**, *26*, 1383.
- [69] S. Kim, M. Lim, *J. Am. Chem. Soc.* **2005**, *127*, 5786.
- [70] S.-Y. Sheu, *J. Chem. Phys.* **2005**, *122*, 901.
- [71] J. Bredenberg, personal communication, **2004**.
- [72] A. Volbeda, E. Garcin, C. Piras, A. L. de Lacey, V. M. Fernandez, E. C. Hatchikian, M. Frey, J. C. Fontecilla-Camps, *J. Am. Chem. Soc.* **1996**, *118*, 12989.
- [73] A. Müller, G. Henkel, *Chem. Commun.* **1996**, 1005.
- [74] A. Müller, G. Henkel, *Z. Naturforsch. B* **1995**, *50*, 1464.
- [75] M. Köckerling, G. Henkel, *Z. Naturforsch. B* **1996**, *51*, 178.
- [76] G. Henkel, M. Köckerling, A. Müller, *Bioinorg. Chem.* **1997**, 456.
- [77] K. Schulbert, R. Mattes, *Z. Naturforsch. B* **1994**, *49*, 770.
- [78] T. A. Wark, D. W. Stephan, *Organometallics* **1989**, *8*, 2836.
- [79] F.-F. Jian, K. Jiao, Y. Li, P.-S. Zhao, L.-D. Lu, *Angew. Chem.* **2003**, *115*, 5900; *Angew. Chem. Int. Ed.* **2003**, *42*, 5722–5724; corrigendum: F.-F. Jian, K. Jiao, Y. Li, P.-S. Zhao, L.-D. Lu, *Angew. Chem.* **2004**, *116*, 14; *Angew. Chem. Int. Ed.* **2004**, *43*, 14.
- [80] E. Feller Scott, K. Gawrisch, D. MacKerell Alexander, Jr., *J. Am. Chem. Soc.* **2002**, *124*, 318.
- [81] S. E. Feller, A. D. MacKerell, Jr., *J. Phys. Chem. B* **2000**, *104*, 7510.
- [82] J. Norberg, L. Nilsson, *Biophys. J.* **1998**, *74*, 394.
- [83] T. Moriuchi, K. Yoshida, T. Hirao, *Organometallics* **2001**, *20*, 3101.
- [84] T. Moriuchi, A. Nomoto, K. Yoshida, T. Hirao, *Organometallics* **2001**, *20*, 1008.
- [85] S. I. Kirin, U. Schatzschneider, X. de Hatten, T. Weyhermüller, N. Metzler-Nolte, *J. Organomet. Chem.* **2006**, *691*, 3451.
- [86] A. Volbeda, J. C. Fontecilla-Camps, *Dalton Trans.* **2003**, 4030.
- [87] S. Niu, L. M. Thomson, M. B. Hall, *J. Am. Chem. Soc.* **1999**, *121*, 4000.
- [88] L. Barisic, V. Ropic, V. Kovac, *Croat. Chem. Acta* **2002**, *75*, 199.
- [89] A. Shafir, M. P. Power, G. D. Whitener, J. Arnold, *Organometallics* **2000**, *19*, 3978.
- [90] L. A. Carpino, G. Y. Han, *J. Org. Chem.* **1972**, *37*, 3404.

Received: March 3, 2007

Revised: June 29, 2007

Published online: August 31, 2007